Edwin I. Hatch Nuclear Plant-Unit 2
Proposed Exemption to 10 CFR 50.46 and
10 CFR 50 Appendix K for HNP Unit 2

Enclosure 9

GNF-0000-0113-8604NP, "GNF-Ziron Performance Benefits and Licensing Requirements Assessment," March 2010
(Nonproprietary)

Global Nuclear Fuel
A Joint Venture of GE,Toshiba, & Hitachi

GNF-0000-0113-8604NP
Class I
March 2010

NON-PROPRIETARY INFORMATION

GNF-Ziron Performance Benefits and Licensing Requirements Assessment

TABLE OF CONTENTS

Page

LIST OF TABLES

LIST OF FIGURES

REVISIONS

Number	Purpose of Revision	Reference
0	Initial issue	

1.0 SUMMARY

GNF has developed a zirconium alloy, designated as GNF-Ziron, which has a demonstrated capability to meet application requirements of components in GNF fuel designs. The primary reason for developing this alloy has been the general trend of the nuclear industry towards higher exposures and the desire to decrease the impact this may have on performance and safety compliance for GNF fuel designs. As such, the focus of this development program has been to identify an alloy capable of meeting or exceeding the performance of Zircaloy, while improving the resistance of fuel components to in-reactor degradation effects, in particular the effects due to absorbed corrosion generated hydrogen.

GNF licenses fuel designs with the NRC based on specific analyses performed using approved methods. Currently, Zircaloy is the zirconium alloy designated for fuel assembly components in licensed GNF fuel designs; for cladding Zircaloy-2 is used. GNF has performed testing and analysis with GNF-Ziron and has determined the performance of GNF-Ziron [[ ]] Zircaloy-2 with respect to design criteria, including thermal-mechanical performance, general corrosion resistance and simulated accident conditions with the exception that GNF-Ziron has demonstrated a [[ ]] Zircaloy-2, within limited data, is with respect to hydrogen absorption and hence ductility.

In a separate document [Reference 1], the processing and metallurgical properties of GNF-Ziron are discussed in more detail. That document also describes properties of GNF-Ziron that [[ ]] Zircaloy. In the following section of this document, the known benefits of GNF-Ziron in areas of hydriding and corrosion are described. Assessments of compliance with design criteria under steady state, anticipated operational occurrences, postulated loss-of-coolant-accident and reactivity insertion accident conditions are provided in this document. The thermal-mechanical performance assessment is conducted with reference to the approved PRIME model and its application methodology [Reference 2].

It is concluded that methodologies, such as PRIME, can be applied to GNF-Ziron without any adverse impact.

2.0 GNF-ZIRON CHARACTERISTICS AND EXPERIENCE

2.1 GNF-ZIRON CHARACTERISTICS

GNF-Ziron (previously described as High Fe Zircaloy-2) is the outcome of many years of research for an improved material for use as cladding and fuel assembly components in BWRs. The primary objective of this research has been to identify an alloy with good corrosion resistance and reduced hydriding characteristics.

The chemical composition of GNF-Ziron is very similar to that of Zircaloy-2. GNF-Ziron has a Fe specification of [[ ]], which is based on a nominal composition of [[ ]] manufacture tolerance. The concentrations of other elements remain unchanged relative to Zircaloy-2. The Fe specification for GNF-Ziron is slightly higher than the upper limits for Zircaloy-2 and Zircaloy-4 (0.20 and 0.24 wt%, respectively). Like Zircaloy-2 currently used by GNF, GNF-Ziron is manufactured from sponge zirconium produced from the Kroll process. GNF plans to use the same manufacturing process to produce GNF-Ziron fuel assembly components as Zircaloy-2; for cladding, the outer surface will be in the as-polished condition. (See reference [1] for more detailed description.)

Because the compositional change is quite small and the same manufacturing process is used, the resultant metallurgical structures (grain shape, grain size, and crystallographic texture) are similar for GNF-Ziron and Zircaloy-2. Consequently, there is little difference in the physical and mechanical properties of GNF-Ziron compared with Zircaloy-2, since such properties are sensitive to changes in metallurgical structure or to large changes in composition.

The second phase precipitates (SPPs) in GNF-Ziron also have similar atomic structure and size distribution as similarly processed Zircaloy-2. The composition change relative to Zircaloy-2 does result in a difference in the composition and number density of the SPPs in GNF-Ziron. These change are minor and do not affect mechanical properties. The change in SPP composition and number density is likely, in principle, to affect the corrosion behavior. However, observations from in-reactor operation have [[ ]] between GNF-Ziron and Zircaloy-2, although there are several indications that show [[ ]] for GNF-Ziron [[ ]]. The corrosion behavior of GNF-Ziron, compared with Zircaloy-2, is discussed further in section 2.4. The only known effect resulting from the compositional difference between GNF-Ziron and Zircaloy-2 appears to be in the absorption of corrosion released hydrogen, as discussed in Section 2.3. The improvement is most evident after long irradiation periods, when most SPPs are dissolved. The available information thus suggests that the change in the composition and number density of the SPPs relative to Zircaloy-2 is [[ ]] that could be providing the improvement in hydrogen absorption. A possible explanation for the reduced hydrogen absorption is that the [[ ]].

2.2 TESTING & OPERATING EXPERIENCE

Following laboratory testing during the 1980's, GNF-Ziron has been exposed to a number of in-reactor evaluations including the Advanced Test Reactor (ATR), the plant C in the US, the Halden test reactor in Norway, the plant K in Japan, and the BOR-60 test reactor in Russia. As summarized in Figure 2-1, the general corrosion behavior was first evaluated in plant C, followed by irradiation at Halden with a variety of water chemistry conditions. The corrosion and hydriding characteristics were further assessed in the plant K. The plant K program included an extensive assessment of the mechanical properties and microstructural evolution of unfueled cladding manufactured from GNF-Ziron. The irradiation programs at the ATR and the BOR-60 addressed the irradiation growth behavior for GNF-Ziron. The performance of this alloy under simulated accident conditions has also been assessed in Japan and at the Argonne National Laboratory (ANL). Lead Use Assemblies (LUAs) consisting of fuel rods, water rods, and spacers manufactured from GNF-Ziron were irradiated in plant G in Europe starting in 1999, reaching ~67 GWd/MTU bundle-averaged exposures in October of 2005. LUA performance was assessed periodically during operation using poolside inspection. Following discharge in 2005, selected rods were sent to a hot cell for more detailed evaluation. In a continuation of this LUA program, two of the GNF-Ziron assemblies have been reinserted in 2008 for two additional years of operation.

More recently, LUAs with GNF-Ziron cladding have been initiated at plant V in the summer of 2007 and have completed 1 cycle of operation. Other LUAs with GNF-Ziron are currently operating at plant F (started in summer of 2008) and plant H (started in spring of 2009). Additionally, channels manufactured from GNF-Ziron have completed two cycles of operation at the plant P (started in Spring 2005) and at plant N (started in Spring 2006) reactors in the US. The results from the testing and LUA programs are discussed in relevant portions of this document and also in Reference [1].

2.3 BENEFIT OF GNF-ZIRON: HYDROGEN ABSORPTION

The hydrogen absorption and associated corrosion behavior of GNF-Ziron, and comparison with Zircaloy-2, is assessed from the irradiation program at plant K. The irradiation program included the evaluation of unfueled GNF-Ziron and Zircaloy-2 cladding to high exposures using dummy neutron source holders in a commercial reactor. The evolution of hydrogen content in GNF-Ziron with fast neutron fluence is shown in Figure 2-2. The results show that, up to 4 cycles (~14 months per cycle), the hydrogen content remains relatively low and there is little difference between GNF-Ziron and Zircaloy-2. After 6 cycles of irradiation, at [[ ]], both GNF-Ziron and Zircaloy-2 showed significant increase in absorbed hydrogen. The increase in absorbed hydrogen at these fluences remains lower for GNF-Ziron compared with Zircaloy-2.

A similar trend with exposure is observed for corrosion weight gain, Figure 2-3. For both GNF-Ziron and Zircaloy-2, corrosion weight gain increases gradually and remains generally low up to 4 cycles of operation and increases substantially on going to 6 cycles. One important difference between corrosion weight gain and hydrogen absorption is that GNF-Ziron and Zircaloy-2 both show similar increase corrosion weight gain at higher exposures, but GNF-Ziron shows significantly lower hydrogen absorption

at higher exposures. The reduced hydrogen absorption in GNF-Ziron at comparable corrosion weight gains, is evident from the hydrogen versus weight gain plot shown in Figure 2-4.

Figure 2-2 through 2-4 collectively indicate that the hydrogen pickup percentage or fraction for GNF-Ziron is lower than Zircaloy-2 at high exposure, as shown in Figure 2-5. In Figure 2-5, GNF-Ziron also shows lower pickup fraction at all tested fluence levels; however, the difference at less than [[ ]] is likely not significant since the corrosion weight gain for these cases, Figure 2-3, is low for both alloys and the pickup fraction is subject to large uncertainties.

In Figure 2-2 to Figure 2-5, the [[ ]] Zircaloy-2 samples covered fast neutron fluence range of between [[( ]] GNF-Ziron covered [[ ]]). This range in fluence level [[ ]] provides an insight into the behavior for Zircaloy-2. Figure 2-2 shows that at the low fluence level, [[ ]], Zircaloy-2 showed elevated hydrogen concentration even though the fluence was less than that [[ ]] reached after [[ ]] of irradiation. The implication is that the increase in hydrogen absorption at high exposure is not simply related to [[ ]]. The data for Zircaloy-2 suggest that [[ ]] was needed to induce the large increase in corrosion weight gain and hydrogen absorption, and that, once the increase starts, [[ ]]. The description for the increase in corrosion and hydrogen content at high exposure for Zircaloy-2 is consistent with other observations reported in the literature [Reference 3]. In summary, the irradiation program from plant K shows that GNF-Ziron behaves similarly to Zircaloy-2 with respect to corrosion, including increased corrosion at high exposure/residence time; however, GNF-Ziron shows a reduced tendency to hydrogen absorption when corrosion increases.

GNF's experience with hydrogen in water rods is consistent with the data from plant K and a similar increase in hydrogen content is observed in water rods at high exposures. Figure 2-6 shows hydrogen content in Zircaloy-2 water rods together with data from the irradiation program at plant K, which were based on non-fueled cladding. Figure 2-6 includes hydrogen data for GNF-Ziron and companion Zircaloy-2 water rods from the LUA program at plant G. The water rod hydrogen data indicates a significant increase in hydrogen content in Zircaloy-2 water rods could occur [[ ]] of in-reactor operation in a reference US plant. However, water rods after [[ ]] at plant G showed low levels of hydrogen without indications of increased hydriding for both GNF-Ziron and Zircaloy-2. A possible explanation is in the plant condition, such as water chemistry, between the reference US plant and plant G in Europe, such that [[ ]] resulted in increased Zircaloy-2 corrosion in the reference US plant but not in plant G. The increased corrosion in the reference US plant resulted in increased hydrogen absorption, as was observed in the irradiation program from plant K. At plant G, both Zircaloy-2 and GNF-Ziron water rods have not undergone increased corrosion; consequently, hydrogen content remains low for both alloys.

The hydrogen contents in the main heat-generating portion of Zircaloy-2 and GNF-Ziron cladding [[ ]] as a function of residence time is shown in Figure 2-7. The data for Zircaloy-2 were obtained from different fuel designs involving different clad thicknesses. Since absorbed hydrogen in cladding is the result of surface corrosion, the hydrogen concentration will be dependent on the clad thickness. In order to compare the hydrogen content for the same clad thickness, the hydrogen

contents shown have been normalized to the nominal GE14 cladding thickness of 26 mils. Compared with Figure 2-6, the hydrogen content in cladding is lower than that in water rods with similar residence time. This difference is consistent with reduced hydrogen absorption due to the temperature gradient across the cladding in the heat-generating portion of the cladding. As with hydrogen in water rods, a significant increase after [[ ]] is evident. Figure 2-7 provides a GNF-Ziron vs. Zircaloy-2 comparison of cladding from the LUA program at plant G after [[ ]] irradiation. Hydrogen data were obtained from 5 GNF-Ziron fuel rods in two assemblies and from 3 Zircaloy-2 fuel rods from one assembly following discharge at [[ ]] bundle average exposure. Other Zircaloy-2 cladding data in the [[ ]]operating time frame had bundle average exposure ranging between [[ ]] than the LUAs from plant G. Figure 2-7 shows that the cladding hydrogen levels after [[ ]] residence time were generally less than [[ ]] irrespective of the exposure [[ ]], and the increase in hydrogen observed at longer residence time has not yet occurred. The similarity in hydrogen content for similar residence time, but over a wide range of exposure, indicates the dominant effect of time in affecting cladding hydrogen pickup. A significant [[ ]] between GNF-Ziron and Zircaloy-2 cladding at [[ ]] residence time and [[ ]] exposure, consistent with the absence of accelerated hydriding.

Indirect comparison of the hydrogen pickup characteristics of GNF-Ziron relative to Zircaloy-2 has been obtained from the lead use channel program at plant P. In this channel LUA program, [[ ]]GNF-Ziron channels were operated with two levels, or i.e. control groups (CG), of extensive exposure to the control blade during the first cycle of operation. After each of two cycles of operation, channel dimensions were measured on [[ ]] GNF-Ziron channels and on 4 control Zircaloy-2 channels that were operated in symmetric core locations and thus experienced the same control blade exposure and hence expected shadow corrosion. For each channel, the deflection or bow across two pairs of opposing channel faces was measured. From the measured data, the shadow corrosion induced channel bow is deduced by subtracting the calculated bow due to irradiation growth from the measured bow. Based on prior poolside measurements and hotcell investigations, shadow corrosion induced bow has been correlated to the hydrogen differential across the channel [Reference 4], and is thus an indicator of hydrogen absorption, as indicated by the alternate vertical scale in Figure 2-8. For channels operated in one of the control groups, CG2, GNF-Ziron channels appear to show less shadow bow compared with Zircaloy-2 after 1 and 2 cycles; the increase during the second cycle is similar for both alloys as indicated by the slope of the dashed lines in Figure 2-8. For the other control group, CG1, GNF-Ziron and Zircaloy-2 developed similar extent of shadow bow after 1 cycle, being greater than for CG2 and is consistent with the greater exposure to the control blade. However, the increase during the second cycle was substantially greater for Zircaloy-2 channels than GNF-Ziron channels, which had similar increase as the channels in CG2. The large increase for the Zircaloy-2 channels in CG1 is consistent with the recent investigation [5], which confirmed that the hydrogen pickup is not substantial when shadow corrosion is established (in the first cycle) and that there is a substantial increase in hydrogen absorption accompanying relatively minor increases in corrosion during subsequent operations. The absence of such an increase for GNF-Ziron is indicative of a reduced tendency to absorb hydrogen once oxide from shadow corrosion has been developed.

The channel bow data in Figure 2-8 and the hydrogen absorption data from the plant K irradiation program both support the conclusion that GNF-Ziron has a lower hydrogen pickup when there is

increased corrosion; in the plant K case, the corrosion increase is due to long residence time and in the channel case, the increased corrosion is due to shadow corrosion.

2.4 BENEFIT OF GNF-ZIRON: CORROSION

The main difference in material characteristic resulting from the increased iron content in GNF-Ziron relative to Zircaloy-2 appears to be the composition and number density of SPPs. SPP in Zircaloys generally are known to affect the corrosion behavior. Therefore, a difference in corrosion response between GNF-Ziron and Zircaloy-2 can be expected in principle. Laboratory tests, supported by in-reactor performance, have shown that the difference is [[ ]]. In laboratory testing, whether or not a difference is observed is found to be sensitive to the testing condition. In Figure 2-9, the corrosion weight gain data following ASTM G2 corrosion testing (72 hr @ 400°C) is shown as a function of the iron content in GNF-Ziron and Zircaloy-2 cladding. Figure 2-9 shows that there is no sensitivity to the cladding Fe content under this industry standard test condition. A companion set of cladding was tested under 1750 psi (12.1 MPa) pressure at 410°C followed by 520°C. This test condition is routinely used by GNF and is considered to be more severe than the ASTM G2 test and to be a more relevant indicator of nodular corrosion performance in BWRs. The weight gain results, Figure 2-10, show that there is [[ ]] in weight gain (i.e. [[ ]]) as the Fe content increased. It should be noted that all test samples shown in Figure 2-10 did not develop any nodules. The no-nodules performance means that the corrosion performances of Zircaloy-2 and GNF-Ziron are both very good, since no-nodule is the most stringent visual criterion for the 410°C/520°C test, which was developed with correlation to corrosion performance in BWRs. The lack of sensitivity to Fe content in the G2 test and the [[ ]]weight gain with increased Fe content under the more severe 410°C/520°C test collectively indicate [[ ]], i.e. [[ ]] for GNF-Ziron.

In-reactor corrosion performance of GNF-Ziron relative to Zircaloy-2 appears to be consistent with expectations based on the laboratory test results in Figure 2-10. The expectation is therefore for [[ ]]under typical BWR water chemistry conditions; [[ ]].

2.4.1 Corrosion of GNF-Ziron: general corrosion

The general corrosion performance of GNF-Ziron under typical BWR conditions has been obtained from the irradiation program at plant K and from LUA programs at plant G and plant V. The corrosion weight gain for GNF-Ziron and Zircaloy-2 as a function of fast neutron fluence from the plant K program is shown in Figure 2-3. As noted earlier, GNF-Ziron and Zircaloy-2 show a similar trend of increased corrosion weight gain at high exposure and there appears to be little difference between the two alloys.

In the LUAs at plant G and plant V, poolside eddy current (EC) liftoff measurements, shown in Figure 2-11, for GNF-Ziron and companion Zircaloy-2 cladding are consistent with GNF's considerable experience base. EC liftoff measures the gap distance between the eddy current probe and the base metal of the zirconium-based component. EC liftoff therefore measures the combined thickness of the

corrosion layer as well as crud layer that generally form during in-reactor operation. The crud layer thickness is strongly dependent on parameters such as the Fe and Zn concentrations in the reactor water and the local power. In any case, EC liftoff measurements represent a conservative assessment of the cladding corrosion.

From the LUAs at plant G, poolside inspections were performed on GNF-Ziron at various times up to [[ ]] bundle average exposure. At [[ ]], inspections were performed on both GNF-Ziron and Zircaloy-2. Up to [[ ]], the inspection results showed GNF-Ziron to be consistent with GNF's experience base. The comparison at [[ ]] showed that the general corrosion characteristic for GNF-Ziron [[ ]]for Zircaloy-2. Representative pictures of cladding appearance at [[ ]] bundle average exposure is shown in Figure 2-12. Figure 2-12 shows the comparison at elevations away from spacer locations. (Enhanced corrosion or shadow corrosion at spacer locations are discussed in the next sub-section). At these locations, there is [[ ]]appearance between GNF-Ziron and the symmetric Zircaloy-2. Both GNF-Ziron and Zircaloy-2 cladding exhibited some minor level of localized crud spalling (white patches) as shown in Figure 2-12. The spalling is not extensive and is primarily introduced during brushing of the fuel rod prior to the visual inspection.

For the more recently initiated LUA program at plant V, GNF-Ziron and Zircaloy-2 at [[ ]] away from spacers, Figure 2-11, which was pre-dominantly due to crud build up, consistent with the plant water chemistry and measured profilometry. The measurements show that crud build up on cladding [[ ]] for GNF-Ziron and Zircaloy-2. In Figure 2-13, the visual appearances of GNF-Ziron and Zircaloy-2 cladding from symmetric locations in the same assembly is compared. The comparison is for locations away from spacers and shows that GNF-Ziron and Zircaloy-2 [[ ]] in visual appearances was evident. (Enhanced corrosion or shadow corrosion at spacer locations are discussed in the next sub-section).

The plant G LUAs also included GNF-Ziron as the water rod material. Following discharge at [[ ]] bundle average exposure, GNF-Ziron and Zircaloy-2 water rods were sent to the hot cell for destructive evaluation. The corrosion behavior in terms of the average ID, OD and total oxide thicknesses at 6 elevations is shown in Figure 2-14. The results show some axial variations in oxide thickness for both GNF-Ziron and Zircaloy-2. In this comparison, Zircaloy-2 appeared to undergo [[ ]] corrosion on the OD, while ID corrosion for GNF-Ziron appeared [[ ]]. On a rod average basis, the combined OD plus ID oxide thickness was [[ ]]for GNF-Ziron and Zircaloy-2.

In summary, testing up to 5 cycles in plant K and inspections of LUAs in plants G and V up to[[ ]] indicate GNF-Ziron and Zircaloy-2 have [[ ]] away from enhanced or shadow corrosion locations.

2.4.2 Corrosion Benefit of GNF-Ziron: under enhanced corrosion conditions

Improved in-reactor corrosion performance of GNF-Ziron relative to Zircaloy-2 has been observed when i) under shadow corrosion conditions in BWRs and ii) water chemistry has been deliberately adjusted in test reactors.

i) Shadow corrosion related: Near spacer locations, both GNF-Ziron and Zircaloy-2 show presence of enhanced (nodular) corrosion due to "shadow" effects associated with the Inconel spacer. The enhanced corrosion is commonly termed shadow corrosion because the corrosion enhancement on the zirconium alloy is related to the presence of a dissimilar metal, such as stainless steel or Inconel, and the area of enhanced corrosion often resembles the shape, or shadow, of the dissimilar metal. Shadow corrosion is particularly noticeable in the GNF2 and older GE12 fuel designs, which have all Inconel spacers. In other fuel designs that use Zircaloy spacers with Inconel springs, the shadow corrosion affected smaller regions of the cladding in accordance with less Inconel material present.

A GNF-Ziron vs. Zircaloy-2 comparison of shadow corrosion due to spacer springs (alloy X750) from the LUA at plant G after [[ ]] bundle average exposure is shown in Figure 2-15. Both GNF-Ziron and Zircaloy-2 showed limited regions of shadow corrosion. The limited region of shadow corrosion is consistent with the Zircaloy spacers with Inconel springs. The visual comparison in Figure 2-15 does not provide information on the oxide thickness and [[ ]]; both alloys exhibited minor level of spalling.

Water rods of GNF-Ziron and Zircaloy-2 from the LUA program at plant G after [[ ]] bundle average exposure have been examined in the hotcell. The spacer locations near ~36-inch elevation were examined in more detail metallographically as shown in Figure 2-16. To aid the comparison, boxes are drawn on the macroscopic visual pictures in Figure 2-16 to indicate the expected contact region with the Inconel spring. Visually, a large difference between the two alloys is not evident, although enhanced corrosion appears to be less evident for GNF-Ziron. The oxide thickness was measured in several (~12) locations evenly distributed around a quarter ring section of each water rod. Figure 2-16 shows the clear presence of enhanced corrosion for Zircaloy-2. However, such enhanced corrosion appears to be absent in the examined GNF-Ziron section, suggesting an improvement in shadow corrosion response relative to Zircaloy-2.

Further indication of improved shadow corrosion response was obtained from poolside inspection of a LUA at plant V after [[ ]] bundle average exposure. Figure 2-17 shows a comparison of eddy current liftoff traces from a pair of GNF-Ziron and Zircaloy-2 fuel rods that were placed in symmetric locations in the assembly. Liftoff traces for both GNF-Ziron and Zircaloy-2 all showed appreciable crud deposition in the ~10 –30 inch elevation, which determined the values of maximum liftoff away from spacers shown in Figure 2-11 and discussed earlier. The focus in this discussion is on the corrosion enhancement or spikes near spacer locations. Figure 2-17 shows that liftoff traces for Zircaloy-2 were characterized by a consistent presence of liftoff spikes at spacer locations. In comparison, traces for GNF-Ziron showed less prominent spikes. The example traces shown in Figure 2-17 are from one pair of

symmetric GNF-Ziron and Zircaloy-2 fuel rods that were characterized at 45° interval azimuthally. Four other pairs were characterized at 90° interval and showed similar differences between GNF-Ziron and Zircaloy-2. The eddy current liftoff results are consistent with visual examination results. Figure 2-18 shows examples of symmetrically located GNF-Ziron and Zircaloy-2 pairs at different axial elevations. The visual examinations show that, at plant V, shadow corrosion on Zircaloy-2 generally manifest as [[ ]], which in some cases were [[ ]]. GNF-Ziron in comparison generally exhibited [[ ]], indicating a greater resistance to shadow corrosion.

While the exact mechanism for shadow corrosion remains the subject of on-going research, it should be noted that when the phenomenon was first observed, shadow corrosion was described as a form of nodular corrosion [6]. Improved response of GNF-Ziron under shadow corrosion conditions thus implies a [[ ]].

ii) Water chemistry effect: The Halden BWR corrosion loop was used to conduct a series of tests in which the water chemistry was deliberately controlled and varied. The test condition simulated the thermo-hydraulic and nuclear conditions. The tested water chemistry included variations in the oxygen and hydrogen concentrations as well as additives such as Zn and sulfate. The detailed conditions are given in Table 2-1 and the test duration was 100 –140 days. Post irradiation metallographic examination showed that GNF-Ziron and Zircaloy-2 generally developed [[ ]] uniform corrosion oxide; however, under some water chemistry conditions Zircaloy-2 developed some nodules whereas GNF-Ziron did not develop nodules under the same condition. Table 2-1 shows that [[ ]]in the water tended to produce nodules in Zircaloy-2 but not GNF-Ziron, i.e.[[ ]] represented a [[ ]] corrosion environment under which GNF- Ziron was less prone to develop nodules than Zircaloy-2.

Table 2-1 Summary Of Corrosion Oxide Thickness After 100 –140 Day Testing Under Different Water Chemistry Conditions In The BWR Corrosion Loop In The Halden Test Reactor

[[

]]

[[

]]

Figure 2-1 In-Reactor Operational Experience Of GNF-Ziron.

[[

]]

Figure 2-2 Hydrogen Content As A Function Accumulated Fast Neutron Fluence.

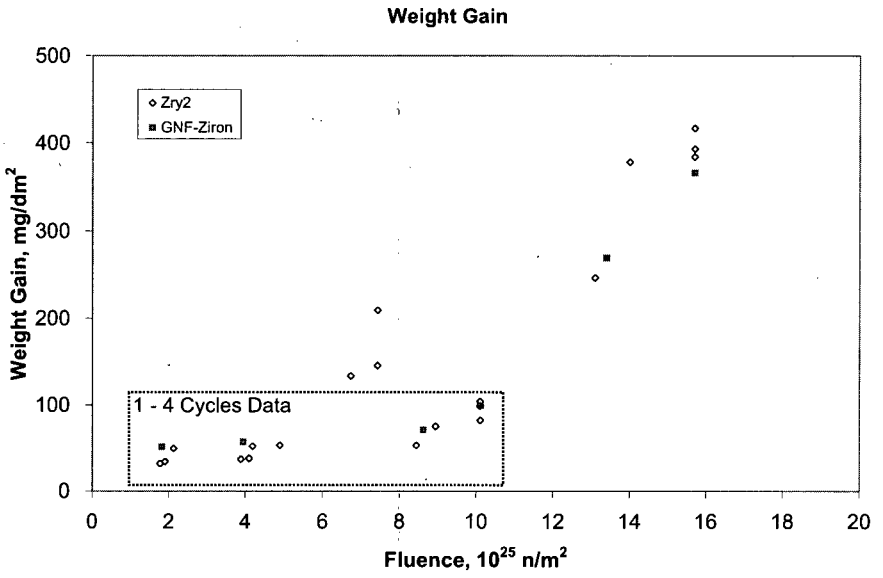

Figure 2-3 Corrosion Weight Gain As A Function Accumulated Fast Neutron Fluence.

[[

]]

Figure 2-4 Hydrogen Concentration As A Function Corrosion Weight Gain.

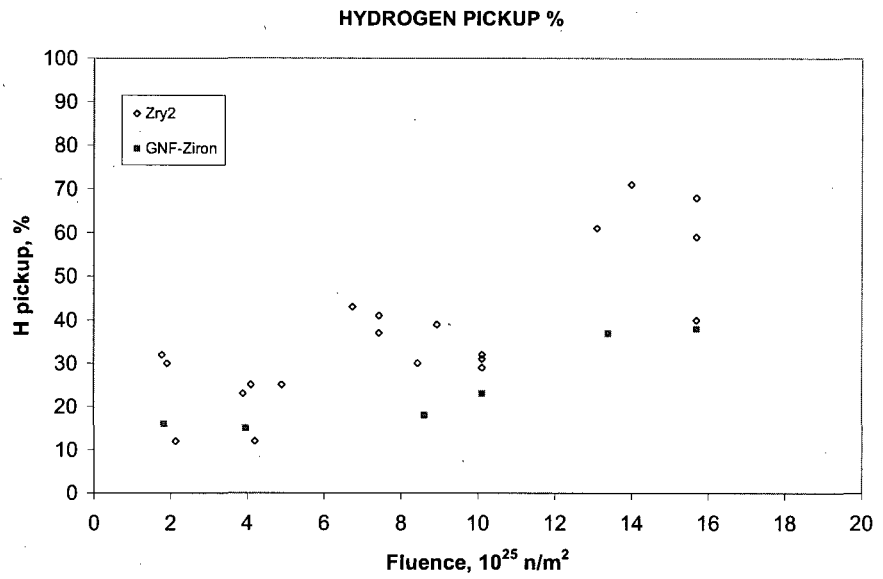

Figure 2-5 Hydrogen Pickup Percentage As A Function Accumulated Fast Neutron Fluence.

[[

]]

Figure 2-6 Hydrogen Concentration In Water Rods And Unfueled Cladding As A Function Of Residence Time.

[[

]]

Figure 2-7 Hydrogen Concentration in Fuel Cladding as a Function of Residence Time for GNF-Ziron (red squares) and Zircaloy-2 (blue diamonds).

[[

]]

Figure 2-8 Shadow Corrosion Bow For GNF-Ziron And Zircaloy-2 Channels After 1 And 2 Cycles Of Operation. Channel Bow Due To Shadow Corrosion Is Related To A Differential In Hydrogen Concentration In Opposite Sides Of A Channel. The Channels Were Operated In Two Sets Of Symmetric Cells, Or Control Groups (CG). CG 1 (Solid Symbols And Line) Has Received Greater Exposure To Control Blade Than CG2 (Open/Dashed Symbols And Line).

[[

]]

Figure 2-9 Corrosion Weight Gain After 72 Hours Autoclave Testing At 400°c For Zircaloy-2 And GNF-Ziron As Function Of Iron Content.

[[

]]

Figure 2-10 Corrosion Weight Gain After Two-Step Test At 410°c/520°c For Zircaloy-2 And GNF-Ziron As Function Of Iron Content.

[[

]]

Figure 2-11 Poolside Eddy Current Liftoff From LUA Programs At Plant G And Plant V. MELO Represents The Maximum Of Running Average Over 6-Inch Axial Length.

[[

]]

Figure 2-12 Comparison Of Visual Appearances Of GNF-Ziron (Lower Row) And Zircaloy-2 (Upper Row) Cladding Away From Spacer Locations After [[ ]] Exposure (Plant G).

[[

]]

Figure 2-13 Comparison Of Visual Appearances Of GNF-Ziron (Lower Row) And Zircaloy-2 (Upper Row) Cladding Away From Spacer Locations After [[ ]] Exposure (Plant V). Each Upper/Lower Pair Is From Similar Axial Elevation In Fuel Rods That Are Symmetric To Each Other In The Fuel Assembly.

[[

]]

Figure 2-14 Metallographic Oxide Thickness In GNF-Ziron And Zircaloy-2 Water Rods After [[ ]] Bundle Average Exposure (Plant G).

[[

]]

Figure 2-15 Comparison Of Visual Appearances Of GNF-Ziron (Lower Row) And Zircaloy-2 (Upper Row) Cladding At Spacer Locations After [[ ]] Bundle Average Exposure (Plant G). Each Upper/Lower Pair Is From Similar Axial Elevation.

[[

]]

Figure 2-16 Visual Appearance Water Rod Made From GNF-Ziron (Right And Zircaloy-2 (Left) At A Spacer Location (~36 Inch Elevation) After [[ ]] Bundle Average Exposure (Plant G). Oxide Thicknesses On Outer Surface Were Measured Metallographicaly Around The Contact Region (Boxes) With The Spacer.

[[

]]

Figure 2-17 Comparison Of Eddy Current Liftoff Traces From A GNF-Ziron (Lower Set In Red) And A Zircaloy-2 (Upper Set In Blue) Cladding In Symmetric Positions Within The Fuel Assembly After [[ ]]Exposure (Plant V). Eight Traces Are Shown For Each Alloy; The Lowermost Trace In Each Set Is Taken At 0° Reference Azimuth And Each Successive Trace Is Taken At 45° To The Previous Trace And Has Been Offset Vertically In Chart For Clarity.

[[

]]

Figure 2-18 Comparison Of Visual Appearances Of GNF-Ziron (Lower Row) And Zircaloy-2 (Upper Row) Cladding At Spacer Locations After[[ ]] Exposure (Plant V). Each Upper/Lower Pair Represents A Comparison At The Same Spacer Location In Fuel Rods In Symmetric Positions Within The Fuel Assembly.

3.0 LICENSING REQUIREMENTS ASSESSMENT

3.1 THERMAL-MECHANICAL

GNF fuel rod design objective is to preclude systematic defects arising under the conditions of authorized operation including normal steady-state operation and anticipated operational occurrences. This fuel rod design objective is achieved by the imposition of mechanistic limits on the predicted performance of the fuel under the conditions of authorized operation. Fuel rod thermal-mechanical performance model PRIME [Reference 2] is applied to provide conservative fuel performance predictions for comparison against the specified performance limits. The material properties of the fuel cladding used in thermal-mechanical design and licensing analyses include:

1. Elastic properties (elastic modulus and Poison's ratio)
2. Thermal expansion coefficients
3. Plastic properties (yield and ultimate stress and failure strain)
4. Creep properties
5. Fatigue properties
6. Irradiation growth properties
7. Corrosion properties

The elastic properties and thermal expansion coefficients are only weakly dependent upon alloy composition and more dependent upon fabrication process, specifically the reduction process and the resulting texture. Since GNF-Ziron has essentially the identical fabrication process and identical texture specifications as the Zircaloy-2 cladding, the minor changes in alloy composition will have negligible impact on these properties and hence on the thermal-mechanical performance of the fuel rods. Likewise, the plastic, creep, fatigue and irradiation growth properties are also only weakly dependent upon alloy composition. However, these properties are strongly dependent upon the fabrication process, specifically the final heat treatment. Since GNF-Ziron cladding are fully recrystallized annealed at the end of the fabrication process, the minor composition changes also have negligible impact on these properties [1]. Finally, the corrosion properties for GNF-Ziron are essentially identical to those of Zircaloy-2 cladding as discussed in Section 2.4 and hence the Zircaloy-2 corrosion rate can be conservatively applied to GNF-Ziron analyses. In addition to the analytical tool, a set of design limits, specifically, *Fuel Rod Internal Pressure, Fuel Melting, Cladding Plastic Strain, Cladding Stress/Strain, Cladding Fatigue, and Cladding Creep Collapse* are applied in the fuel rod thermal-mechanical design analyses, to ensure that fuel rod mechanical integrity is maintained throughout the fuel rod design lifetime. An assessment of the impact of the GNF-Ziron cladding on each of these design and licensing limits along with the applicability of the PRIME models and associated uncertainties are discussed below.

3.1.1 Fuel Rod Internal Pressure

The design and licensing limit on fuel rod internal pressure is that it cannot exceed the value for which the cladding creepout rate becomes equal to the fuel pellet fission product (solid) swelling rate. If the fuel rod internal pressure exceeds the coolant pressure, the resulting cladding tensile hoop stress causes the cladding to deform outward (cladding creepout). If the rate of this cladding outward deformation exceeds the fuel pellet irradiation swelling rate, the pellet-cladding gap will begin to open. An increase in the pellet-cladding gap would reduce the pellet-cladding thermal conductance, thereby increasing the fuel temperature. The increased fuel temperatures would result in further fuel pellet fission gas release, greater fuel rod internal pressure, and, correspondingly, a faster rate of cladding outward deformation and gap opening. A limit on fuel rod internal pressure is applied to prevent this adverse feedback condition.

Conformance to the fuel rod internal pressure design and licensing criterion is performed through the evaluation of a fuel rod internal pressure design ratio, defined as

$$\text{Design Ratio} = \frac{\text{Fuel Rod Internal Pressure}}{\text{Fuel Rod Critical Pressure}}$$

where, the fuel rod critical pressure corresponds to the pressure that would cause the fuel rod to creep out at a rate equal to the instantaneous fuel pellet irradiation swelling rate. The design ratio is evaluated statistically and formulated in such a way that a value of 1.0 provides 95% confidence that the fuel rod internal pressure will not exceed the critical pressure. Therefore, the value of the fuel rod internal pressure design ratio should be maintained ≤ 1.0.

Key cladding properties/phenomena that may impact the compliance with the rod internal pressure limits are cladding creep, conductivity, thermal expansion, and cladding oxidation. Based on the available in reactor creep test data as shown in Reference [1] (Figure B-10), GNF-Ziron has the [[
]]. The minor differences in the Zircaloy-2 and GNF-Ziron creep data are well bounded by the creep rate uncertainty [[
]] applied in the fuel rod internal pressure design ratio calculations. In addition, as discussed in Reference [1] (section B.2) thermal properties (conductivity, thermal expansion, etc.) of Zircaloy-2 are applicable to GNF-Ziron as these properties are not sensitive to the small changes in composition, and as such the PRIME Zircaloy-2 correlations are applicable. The corrosion behavior of GNF-Ziron isessentially identical to that of Zircaloy-2 as discussed in Section 2.4 and such the PRIME oxide rate and initial values can be conservatively applied for GNF-Ziron corrosion behavior modeling. Based on these discussions, it can be concluded that the PRIME Zircaloy-2 models and associated uncertainties conservatively represent the GNF-Ziron behavior and no adverse impact on fuel rod internal pressure design ratio calculations are expected due to the application of GNF-Ziron cladding.

3.1.2 Fuel Melting

The design and licensing limit on fuel temperature is that the maximum fuel centerline temperature cannot exceed the fuel melting temperature during normal operation, including anticipated operational occurrences (AOOs). This fuel temperature limit is applied to ensure that sudden shifting of molten fuel in the interior of the fuel rods, and subsequent potential cladding damage, is precluded.

The PRIME model and its associated application methodology determines the Thermal Overpowers (TOP) limit in terms of LHGR to assure with 95% confidence that fuel melting will not occur. Except for the fuel properties, cladding corrosion performance has the potential of impacting fuel melt margin. If the cladding is oxidized at a faster rate, then the thick oxide layer at the cladding outer surface will act as a barrier for heat transfer from the cladding to the coolant. As a consequence, fuel temperature will be higher and margin to fuel melting will be lower. However, as shown in Section 2.4, the corrosion behavior of GNF-Ziron is [[ ]]Zicaloy-2 corrosion data. Moreover, the fuel melting is limited at the beginning of life for the fuel rods, usually at the knee of LHGR limit curve (~16 GWd/MTU), where GNF-Ziron's corrosion performance is [[ ]] Zircaloy-2. Thus, it can be concluded that the PRIME Zircaloy-2 models can be conservatively applied for GNF-Ziron behaviors modeling and no adverse impact on fuel melting is expected for the GNF-Ziron cladding.

3.1.3 Cladding Plastic Strain

The design and licensing limit on cladding strain is that the [[

]] These limits are applied to ensure that fuel rod failure due to pellet-cladding mechanical interaction will not occur.

Like the thermal overpower (TOP) limit, a mechanical overpower limit (MOP) is defined to protect against the [[ ]] plastic strain. This overpower limit (MOP) is applied at the most limiting exposure to calculate the cladding permanent strain (plastic plus creep) and compared against the licensing limit. All the evaluations for cladding permanent strain are performed using [[ ]] basis for fuel rod design parameters as opposed to the [[ ]] used for other criteria. It is noted that stress strain relationship for GNF-Ziron material is [[ ]] to Zircaloy-2 as shown in Reference [1]. Moreover, cladding ductility is a function of fluence and hydrogen content and Section 2.3 indicates GNF-Ziron has a potentially lower hydrogen pickup than Zircaloy-2, even at lower fluences. Thus, this assessment concludes that GNF-Ziron doesn't constitute any adverse impact on the [[ ]] plastic strain limit.

3.1.4 Cladding Stress/Strain

The fuel assembly components are evaluated to ensure that the fuel will not fail due to stresses or strains exceeding the fuel assembly component mechanical capability. The fuel rod stress analysis was

performed using a Monte Carlo statistical method to calculate the effects of pressure differential, cladding ovality, radial thermal gradients, spacer contact, thermal bow and circumferential thermal gradients. The calculated stresses are compared with the appropriate design limit to produce a design ratio. Design ratios of less than 1.0 provide 95% confidence that the fuel will not fail due to stresses or strains exceeding the fuel assembly component mechanical capability.

As reported in Reference [1], GNF-Ziron ductility [[ ]] to Zircaloy-2 as represented by the total elongation and reduction in area. As a result, the microscopic or local strain to failure for GNF-Ziron is [[ ]] for Zircaloy-2. Therefore, no adverse effect on cladding stress/strain limit is expected for GNF-Ziron.

3.1.5 Cladding Fatigue

Fuel rod cladding is evaluated to ensure that strains due to cyclic loadings will not exceed the fatigue capability of the cladding material. The cladding strain cycles are analyzed using the rain flow cycle counting method. The fractional fatigue life expended for each strain cycle is determined and summed over the total number of cycles to determine the total fatigue life expended over the fuel design lifetime. The calculated upper 95% total fatigue life expended are compared with the design limit which requires that the total accumulated fractional fatigue life expended be <1.0.

Reference [1] shows no significant difference in fatigue behavior between Zircaloy-2 and GNF-Ziron. Also for a given strain amplitude, the number of cycles to failure is larger for GNF-Ziron than that can be resulted from GEH/GNF design curve. Therefore, for fuel with GNF-Ziron cladding loss of mechanical integrity due to cladding fatigue is not expected.

3.1.6 Cladding Creep Collapse

The fuel rod is evaluated to ensure that fuel rod failure due to cladding collapse into a fuel column axial gap will not occur. Such collapse occurs due to a slow increase of cladding initial ovality caused by creep from the combined effect of reactor coolant pressure, temperature and fast neutron flux on the cladding over the axial gap. This condition occurs at cladding stress levels far below that required for elastic buckling or plastic deformation. As noted before, GNF-Ziron creep strength is similar to Zircaloy-2. Thus, it can be concluded that failure due to cladding creep collapse is not expected for fuel rods with GNF-Ziron cladding.

3.2 POSTULATED LOSS-OF-COOLANT ACCIDENT (LOCA)

3.2.1 Current Criteria

10 CFR Part 50.46, "Acceptance criteria for emergency core cooling systems for light-water nuclear power reactors," requires that the calculated emergency core cooling system (ECCS) performance for reactors with Zircaloy or ZIRLO fuel cladding meet certain criteria. 10 CFR Part 50 Appendix K, "ECCS Evaluation Models," further requires that the Baker-Just (BJ) equation be used in the ECCS evaluation model to determine the rate of energy release, cladding oxidation, and hydrogen generation after a

postulated loss-of-coolant accident (LOCA). The BJ equation presumes the use of Zircaloy or ZIRLO fuel cladding. The composition of GNF-Ziron is outside of the composition range defined in ASTM industry standards for Zircaloys. Since there is no provision for cladding material other than Zircaloy or ZIRLO in 10 CFR 50.46 and Part 50 Appendix K, the use of GNF-Ziron as the cladding material will therefore require exemptions to the current 10 CFR 50.46 and Part 50 Appendix K.

10 CFR 50.46 has requirements related to the maximum cladding oxidation, peak cladding temperature, maximum hydrogen generation, coolable geometry and long-term cooling. High temperature oxidation tests have been conducted on GNF-Ziron as discussed in section B.5 of Reference [1]. Specifically, the oxidation kinetics data at 1000°C (1273 K) and 1200°C (1473 K) shown in Figures B-13 and B-14 of Reference [1] show the oxidation data for GNF-Ziron to be consistent or conservative relative to predictions based on the Cathcart-Pawel (CP) relationship. At these temperatures, the BJ relationship generally predicts more oxidation that the CP relationship. Therefore, the use of the BJ equation remains conservative in the postulated LOCA circumstances relative to the measured GNF-Ziron data.

The maximum cladding oxidation and peak cladding temperature limits are collectively known as the embrittlement criteria. In order to address the potential embrittlement due to cladding oxidation associated with a postulated LOCA, ring compression tests were conducted to determine the post-test ductility following oxidation at 1000°C and 1200°C. The resultant post-quench ductilities (based on offset strain) as a function of ECR shown in Figures B-16 and B-17 of Reference [1] show that the embrittlement ECR is compliant with the current 17% ECR criterion. It should be noted that the ECR values in Reference [1] are expressed using the CP correlation, whereas the current embrittlement criterion is based on BJ equation. If the BJ equation was used, the embrittlement ductilities for GNF-Ziron would be higher than indicated in Figures B-16 and B-17 (based on offset strain) or in Figures B-18 and B-19 (based on permanent strain) of Reference [1]. The test results thus indicate margin to embrittlement relative to the 17% ECR clad oxidation limit stated in 10 CFR 50.46. As discussed in section B.5.b of Reference [1], additional quench tests under a restraining load have been conducted. The test results showed ductility up to [[ ]] ECR based on BJ. Although these tests differ from the ring-compression testing that forms the basis of the post-quench ductility criteria in 10 CFR 50.46, these results provide additional assurance that adequate post-quench ductility in the GNF-Ziron cladding material will be maintained.

The iron content of GNF-Ziron deviates only slightly from that of Zircaloy-2, while the alloy compositions are otherwise the same. Consequently, a significant change in the hydrogen generated from cladding-water reaction is not expected. Additionally, since the composition change is only increased Fe content relative to Zircaloy-2, the change in essence replaces some zirconium atoms with iron atoms. The potential effect on hydrogen generation due to replacing one Zr atom with a Fe atom can be estimated as follows. Each Zr atom will react with two H_2O molecules to form stoichiometric ZrO_2, thereby releasing 4 hydrogen atoms. Since Fe has a lower valence than Zr, each Fe atom can result in the release of 2, 3, or 2.67 atoms of hydrogen depending on whether stoichiometric Fe0, Fe_2O_3 or Fe_3O_4, respectively, is formed from the reaction with water. The expected result of replacing one Zr atom with one Fe atom is therefore a reduction in the number of released hydrogen atoms. Thus, because of the similarity in composition between Zircaloy-2 and GNF-Ziron, evaluation of hydrogen release based on GNF-Ziron cladding is

conservatively bounded by the calculation based on Zircaloy-2 cladding, and any difference in calculated hydrogen generation would be slightly less for the GNF-Ziron case.

A comparison of test data obtained from GNF-Ziron with available data for Zircaloy is shown in Figure B-6 of Reference [1], which shows that the high temperature perforation characteristics for GNF-Ziron [[

]] and because of the similar composition and similar response to similar fabrication process.

The similarity in composition with Zircaloy-2 and the high temperature test results described above thus demonstrate with a high degree of confidence that, with the exception of not being Zircaloy or Zirlo, the requirements currently in 10 CFR 50.46 and Part 50 Appendix K are met when GNF-Ziron is used as the cladding material. Therefore, there is no anticipated decrease in coolability or increase in dose consequences as a result of a postulated LOCA for GNF-Ziron relative to evaluations performed assuming Zircaloy cladding.

3.2.2 Likely Future Criteria

The US NRC is currently in the process of revising 10 CFR 50.46(b) Reference [7]. The specific details of the revision have not been finalized. The likely key changes are the switch to a set of non-alloy-specific performance-based criteria, use of CP equation for ECR evaluation, addressing the potential for breakaway oxidation, setting of hydrogen (exposure) dependent ECR limit, and accounting for oxidation on clad inner surface in high exposure fuel.

The switch to performance-based criteria will allow alloys such as GNF-Ziron to be more readily introduced as fuel cladding material. The high temperature oxidation characteristics compared with BJ and CP predictions are shown in Figures B-13 to B-15 of Reference [1] and it is evident that the CP equation provides a better representation for GNF-Ziron behavior than BJ. The consistency of these doubled-sided oxidation results between GNF-Ziron and Zircaloy-2 imply that the inclusion of double-sided oxidation to account for inner surface oxidation in high exposure fuel would have the same applicability for the two alloys. The high temperature oxidation tests also serve the purpose of assessing the breakaway oxidation behavior. The results (Figures B-13 and B-15 of Reference [1]) confirm that breakaway oxidation at 1000°C had not occurred up to 5000 seconds, the longest time investigated and of interest for postulated LOCA considerations. The post-quench ductility data, shown in Figures B-16 to B-19 of Reference [1], show that GNF-Ziron meets the CP-based 17% ECR embrittlement criterion (based on either 2% offset strain or 1% permanent strain) in the as-fabricated state. With respect to the hydrogen dependent ECR limit after irradiation, the data generated in Reference [8] from various irradiated cladding alloys (Zircaloy-4, Zirlo and M5) are expected to be applicable to GNF-Ziron (and Zircaloy-2), since the results reflect a generic, alloy independent hydrogen effect. In Figure 2-7, the hydrogen content in Zircaloy-2 cladding is shown as function of residence time. In the [[ ]] time frame, cladding hydrogen data obtained from fuel assemblies with between [[ ]] bundle average exposure typically showed less than [[ ]] at axial elevations [[ ]], which represent the main heat generating portion of the fuel rod. Up to these levels of hydrogen, Figures 236 and 237 in reference [8] show that only a minor adjustment (lowering) in the

maximum ECR would be needed. The data in Figure 2-7 specific to GNF-Ziron were obtained after [[ ]] bundle average exposure and are consistent with the hydrogen content in companion Zircaloy-2 cladding. It is possible that at long residence times, Zircaloy-2 may show higher H than in Figure 2-7, but GNF-Ziron is expected to show lower H than Zircaloy-2 in these situations.

Although the revision to 10 CFR 50.46(b) is not yet complete, the high temperature test results described above thus demonstrate with a high degree of confidence that the requirements likely to be in the revised 10 CFR 50.46 would be met when GNF-Ziron is used as the cladding material.

3.3 REACTIVITY INSERTION ACCIDENT (RIA)

Current criteria related to RIA have limits that address radiological consequences due to fuel cladding failure and core coolability. On cladding failure, current critria for failure for Control Rod Drop Accident (CRDA) for BWRs are a) radial average fuel enthalpy greater than 170 cal/g at zero or low power, and b) local heat flux exceeding fuel thermal design limits for at-power events. On core coolability, current critria are a) fuel radial average energy density not exceeding 280 cal/g, and b) reactor pressure limited to be less than that causing stresses to exceed Service Level C of ASME Boiler and Pressure Vessel code. A revision to the RIA criteria is currently in progress and an interim set of acceptance criteria for RIA have been issued, Reference [9]. The interim criteria addressing cladding failure are

a) for zero power conditions, peak radial average fuel enthalpy greater than 170 cal/g for fuel rods with an internal rod pressure at or below system pressure and 150 cal/g for fuel rods with an internal rod pressure exceeding system pressure; for intermediate and full power conditions, fuel cladding is assumed to be failed if local heat flux exceeds thermal design limits and

b) for BWRs, radial average fuel enthalpy greater than the hydrogen-dependent limits, in which the limiting radial average fuel enthalpy is lowered from 150 cal/g at 75 ppm hydrogen in cladding to 60 cal/g at 150 ppm hydrogen and greater.

On core coolability, the interim critria are:

a) Peak radial average fuel enthalpy must remain below 230 cal/g,

b) Peak fuel temperature must remain below incipient fuel melting conditions,

c) Mechanical energy generated as a result of (a) non-molten fuel-to-coolant interaction and (b) fuel rod burst must be addressed with respect to reactor pressure boundary, reactor internals, and fuel assembly structural integrity, and

d) No loss of coolable geometry due to (a) fuel pellet and cladding fragmentation and dispersal and (b) fuel rod ballooning.

The current criteria are addressed through core design and energy deposition calculation. There is no requirement for specific inputs for clad type or properties. It is understood that mechanical properties of the cladding have been embodied within the enthalpy-based criteria. Since the mechanical properties of GNF-Ziron are indistinguishable from those for Zircaloy-2 (Section B.3 of Reference [1]), the approach used for Zircaloy-2 would be applicable to GNF-Ziron. Therefore, GNF-Ziron clad complies with current criteria by following the same energy deposition based approach to core design.

The interim criteria introduce a failure criterion that is dependent on the hydrogen content of the cladding. The criterion is not alloy specific, since the hydrogen content is the primary factor of interest. In other words, the response of different Zr-based cladding alloys is dependent on the hydrogen content rather than mechanical properties of each alloy. This is because under the conditions of interest, most Zr-based alloys behave similarly, dominated by hydrogen effects. GNF-Ziron can therefore meet the same hydrogen content-based failure criteria in the same manner as Zircaloy-2. The corrosion and hydriding characteristics that lead up to hydrogen accumulation in the cladding is discussed in Sections 2.3 and 2.4 and the mechnical properties in Reference [1].

4.0 REFERENCES

[1] "GNF-Ziron Basic Characteristics and Properties", GNF-0000-0101-6839P

[2] "The PRIME Model for Analysis of Fuel Rod Thermal – Mechanical Performance", NEDC-33256P.

[3] T. Miyashita et al, "Corrosion And Hydrogen Pick-Up Behaviors Of Cladding And Structural Components In Bwr High Burnup 9x9 Lead Use Assemblies", Proceedings of the 2007 International LWR Fuel Performance Meeting, San Francisco, California, September 30 – October 3, 2007

[4] S. T. Mahmood et al, "Channel Bow in Boiling Water Reactors – Hot Cell Examination Results and Correlation to Measured Bow", Proceedings of the 2007 International LWR Fuel Performance Meeting, San Francisco, California, September 30 – October 3, 2007

[5] S.T. Mahmood et al, "Shadow Corrosion-Induced Bow Of Zircaloy-2 Channels", in *Zirconium in the Nuclear Industry – Sixteenth International Conference*, 2010.

[6] F.W. Trowse et al, "Nodular Corrosion Of Zircaloy-2 And Some Other Zirconium Alloys In Steam Generating Heavy Water Reactors And Related Environments", in *Zirconium in the Nuclear Industry – Third International Conference*, ASTM STP 633, 1977, p 236.

[7] Advance Notice of Proposed Rulemaking, 10 CFR Part 50 Performance-Based Emergency Core Cooling System Acceptance Criteria, Federal Register Vol. 74, No. 155, 2009.

[8] NUREG/CR-6967, ANL-07/04, "Cladding Embrittlement During Postulated Loss-of-Coolant Accidents"

[9] NUREG-0800, US-NRC Standard Review Plan, 4.2 Fuel System Design, rev 3, March 2007.